PSI-SR-1242

The electric oxygen-iodine laser: Chemical kinetics of $O_2(a^1\Delta)$ production and $I(^2P_{1/2})$ excitation in microwave discharge systems

W.T. Rawlins
S. Lee
W.J. Kessler
D.B. Oakes
L.G. Piper
S.J. Davis

LASE 2006

High Energy/Average Power Lasers and Intense Beam Applications

21 – 26 January 2006

San Jose, CA

Report Documentation Page

Form Approved
OMB No. 0704-0188

1. REPORT DATE	2. REPORT TYPE	3. DATES COVERED
JAN 2006		**00-00-2006 to 00-00-2006**

4. TITLE AND SUBTITLE	5a. CONTRACT NUMBER
The electric oxygen-iodine laser: Chemical kinetics of O2(a1) production and I(2P1/2) excitation in microwave discharge systems	5b. GRANT NUMBER
	5c. PROGRAM ELEMENT NUMBER
6. AUTHOR(S)	5d. PROJECT NUMBER
	5e. TASK NUMBER
	5f. WORK UNIT NUMBER
7. PERFORMING ORGANIZATION NAME(S) AND ADDRESS(ES) **Physical Sciences Inc,20 New England Business Center,Andover,MA,01810**	8. PERFORMING ORGANIZATION REPORT NUMBER
9. SPONSORING/MONITORING AGENCY NAME(S) AND ADDRESS(ES)	10. SPONSOR/MONITOR'S ACRONYM(S)
	11. SPONSOR/MONITOR'S REPORT NUMBER(S)

12. DISTRIBUTION/AVAILABILITY STATEMENT
Approved for public release; distribution unlimited

13. SUPPLEMENTARY NOTES
The original document contains color images.

14. ABSTRACT

15. SUBJECT TERMS

16. SECURITY CLASSIFICATION OF:			17. LIMITATION OF ABSTRACT	18. NUMBER OF PAGES	19a. NAME OF RESPONSIBLE PERSON
a. REPORT	b. ABSTRACT	c. THIS PAGE			
unclassified	**unclassified**	**unclassified**		**15**	

The electric oxygen-iodine laser: Chemical kinetics of $O_2(a^1\Delta)$ production and $I(^2P_{1/2})$ excitation in microwave discharge systems

W.T. Rawlins*, S. Lee, W.J. Kessler, D.B. Oakes, L.G. Piper, and S.J. Davis
Physical Sciences Inc., 20 New England Business Center, Andover, MA, USA 01810-1077

ABSTRACT

Generation of singlet oxygen metastables, $O_2(a^1\Delta)$, in an electric discharge plasma offers the potential for development of compact electric oxygen-iodine laser (EOIL) systems using a recyclable, all-gas-phase medium. The primary technical challenge for this concept is to develop a high-power, scalable electric discharge configuration that can produce high yields and flow rates of $O_2(a)$ to support $I(^2P_{1/2}\rightarrow{}^2P_{3/2})$ lasing at high output power. This paper discusses the chemical kinetics of the generation of $O_2(a)$ and the excitation of $I(^2P_{1/2})$ in discharge-flow reactors using microwave discharges at low power, 40-120 W, and moderate power, 1-2 kW. The relatively high E/N of the microwave discharge, coupled with the dilution of O_2 with Ar and/or He, leads to increased $O_2(a)$ production rates, resulting in $O_2(a)$ yields in the range 20-40%. At elevated power, the optimum $O_2(a)$ yield occurs at higher total flow rates, resulting in $O_2(a)$ flow rates as large as 1 mmole/s (~100 W of $O_2(a)$ in the flow) for 1 kW discharge power. We perform the reacting flow measurements using a comprehensive suite of optical emission and absorption diagnostics to monitor the absolute concentrations of $O_2(a)$, $O_2(b)$, $O(^3P)$, I_2, $I(^2P_{3/2})$, $I(^2P_{1/2})$, small-signal gain, and temperature. These measurements constrain the kinetics model of the system, and reveal the existence of new chemical loss mechanisms related to atomic oxygen. The results for $O_2(a)$ production at 1 kW have intriguing implications for the scaling of EOIL systems to high power.

Keywords: Electrically pumped oxygen iodine laser, closed cycle laser, singlet oxygen, chemiluminescence

1. INTRODUCTION

The Electric Oxygen Iodine Laser (EOIL) uses an electric discharge of a flowing oxygen gas mixture to generate singlet oxygen metastables, $O_2(a^1\Delta_g)$, and atomic oxygen, which subsequently react with molecular iodine to excite the atomic iodine lasing transition, $I(^2P_{1/2}\rightarrow{}^2P_{3/2})$, at 1.315 μm. The viability of EOIL has been recently demonstrated through measurements of positive gain and lasing in low-power laboratory systems.[1-4] The $I(^2P_{1/2})$ (or I*) excitation mechanism in EOIL is similar to that for the Chemical Iodine Oxygen Laser, COIL, except that dissociation of the reagent I_2 occurs through rapid reactions with O rather than the much less efficient energy transfer from $O_2(a)$. COIL systems use an aqueous chemical process to generate $O_2(a)$, so no O is present, and I_2 must be dissociated by a complex multistep process which consumes some of the $O_2(a)$. EOIL's potential for gas-phase electric discharge generation of the active oxygen species offers substantial improvements in efficiency and weight limitations of closed-cycle systems.

The basic EOIL mechanism for the reactions between I_2 and the effluent of the oxygen discharge is:

$O + I_2 \rightarrow IO + I$ $O + IO \rightarrow O_2 + I$	I_2 dissociation
$O_2(a) + I \leftrightarrows O_2(X) + I^*$	I* excitation (near-resonant, reversible)
$O + I^* \rightarrow O + I$	I* quenching

The two dissociation reactions have near gas-kinetic rate coefficients, and rapidly react in less than the reagent mixing time to produce complete dissociation if $[O] > 2[I_2]$. As with COIL, the I* excitation by energy transfer from $O_2(a)$ is near-resonant and reversible; the forward and reverse rate coefficients stand in the ratio of the temperature-dependent equilibrium constant:

* rawlins@psicorp.com; phone 1 978 689-0003; fax 1 978 689-3232; psicorp.com

$$k_f/k_r = K_{eq}(T) = 0.75 \exp(402/T)$$

The quenching of I* by O is not well understood, and may occur through a multistep reaction mechanism; however, the process results in a significant loss of I* (and thereby in $O_2(a)$) for typical discharge-generated O concentrations.[5] Thus it is important to carefully control the O concentration through titrations with NO_2 and/or NO,[1-4] so that [O] is large enough to dissociate I_2 but small enough to minimize I* quenching:

$$O + NO + M \rightarrow NO_2 + M$$
$$O + NO_2 \rightarrow NO + O_2$$

(Additional reactions involving discharge-generated O_3 are possible, but are not likely to contribute owing to the low concentrations expected for O_3. Further investigations are in progress to test this contention.)

The I* excitation mechanism results in a rate law of the form

$$d[I^*]/dt = k_f[O_2(a)][I] - k_r[I^*][O_2(X)] - k_O[I^*][O]$$

where the net effect of I* quenching is to convert $O_2(a)$ to $O_2(X)$ as the reaction time increases. For slow quenching, a quasi-steady state approximation for [I*] gives

$$[I^*]/[I] \cong k_f[O_2(a)] / \{k_r[O_2(X)] + k_O[O]\}$$

As $k_O[O]$ decreases through reduction of [O], $k_O[O] < k_r[O_2(X)]$, the expression approaches a true steady-state relationship,

$$[I^*]/[I] \cong k_f[O_2(a)] / k_r[O_2(X)] = K_{eq}(T)[O_2(a)]/[O_2(X)] \quad (1)$$

This expression defines the maximum [I*]/[I] ratio that can be achieved for a given $[O_2(a)]/[O_2(X)]$ and temperature. Through consideration of the atomic iodine state dynamics and degeneracies, it can be shown that population inversion and positive gain are achieved if [I*]/[I] > 0.5. Thus Eq. (1) can be used to define a minimum $[O_2(a)]/[O_2(X)]$ ratio required to achieve gain.

The total O_2 introduced into the system, $[O_2]_o$, is given by

$$[O_2]_o = [O_2(X)] + [O_2(a)] + [O]/2 \quad (2)$$

The ratio $[O_2(a)]/[O_2]_o$ is then defined as the yield of $O_2(a)$ produced by the discharge, Y_Δ, and is a fundamental metric for the performance of the system. We can combine Eqs. (1) and (2) to define the minimum $O_2(a)$ yield that must be exceeded in order to produce positive gain, in the limit of negligible [O]. The resulting curve is shown in Fig. 1. For a supersonically cooled flow of ~200 K, $Y_\Delta > 8.2\%$ is required to achieve gain. However, in microwave discharge systems in the 0.1-1 kW range, we typically observe $O_2(a)$ yields in the 20-35% range for dilute O_2/rare-gas mixtures, well above threshold even at room temperature. Indeed, for a 70-100 W microwave discharge-flow system, we have observed positive I*→I gain in subsonic flow at 350 K.[4]

The total $O_2(a)$ power produced by the EOIL discharge is the product of the $O_2(a)$ molar flow rate and energy:

$$P_\Delta = F_{O_2} \; Y_\Delta \; E_\Delta$$

where F_{O_2} is the molar flow rate of O_2, Y_Δ is the $O_2(a)$ yield, and E_Δ is $O_2(a)$ energy, 94.369 kJ/mole. An alternative metric, which requires specification of the laser cavity temperature, is the $O_2(a)$ power available above the gain threshold:

$$P_{\Delta,\,avail} = F_{O_2} (Y_\Delta - Y_o(T)) E_\Delta = P_\Delta (1 - Y_o(T)/Y_\Delta) \quad (3)$$

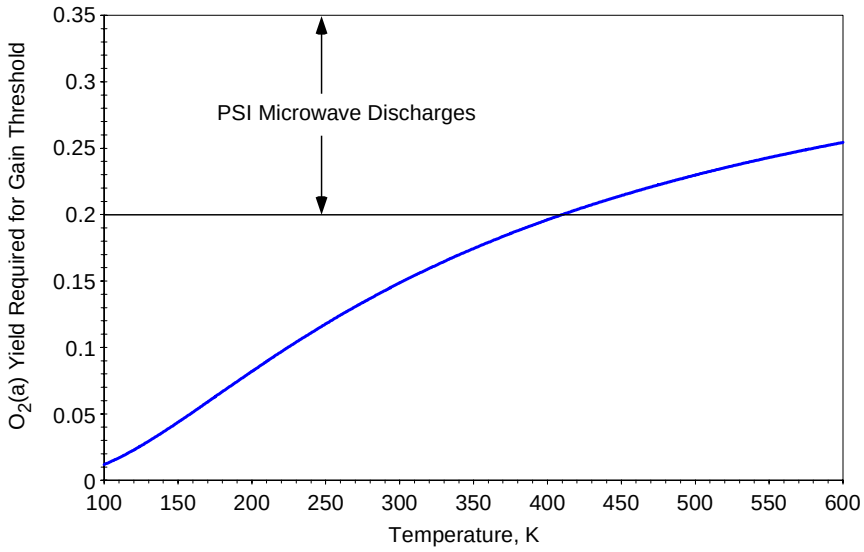

Figure 1: $O_2(a)$ yields required to reach the I*/I transparency threshold, from Eqs. (1) and (2).

where $Y_o(T)$ is the threshold $O_2(a)$ yield as given by Eqs. (1) and (2) and plotted in Fig. 1. The available power is the theoretical maximum that can be extracted as laser power if there are no losses in the system. Typically, $Y_o(T)$ is greatly reduced by supersonic expansion, so the available power increases with decreasing cavity temperature. Limitations of reagent mixing, reaction kinetics, and optical losses will reduce the power extracted in a practical system. However, the total and available $O_2(a)$ power are important figures of merit in the evaluation of EOIL generator performance. Clearly, the performance scales as the product of the $O_2(a)$ yield and the total oxygen flow rate, so both high yields and high gas flow rates are required to scale laser powers into the kW range and higher. For example, if $Y_\Delta \sim 25\%$ and $Y_o(200\ K) \sim 8\%$, then $P_{\Delta,\,avail} \sim (2/3)\ P_\Delta$, so an available laser power of 1 kW would require a total $O_2(a)$ power of 1.5 kW and an oxygen flow rate (in rare gas diluent) of ~0.06 mole/s (80 l/min at STP).

2. DISCHARGE EXCITATION PHENOMENA

$O_2(a)$ can be generated in a variety of electric discharges and configurations. In this work, we have used electrodeless microwave discharges at 2450 MHz. For low-power, room temperature discharge-flow experiments, we use an Evenson-type[6] resonant cavity at 40-120 W power, with flowing O_2/Ar or O_2/He mixtures at pressures of a few torr, and E/N = 50-100 Td.[5,7] For higher power and high throughput, we have implemented a coaxial, 1 kW device at 40-50 torr O_2/He and ~30-40 Td, as described in the next section.

We have previously published model calculations of excitation rates in O_2/Ar discharges.[8] We use a computer code[9] which solves the Boltzmann transport equation.[10] The code treats all the inelastic processes occurring in the active discharge, to evaluate the steady-state electron energy distributions and reaction rate coefficients as functions of E/N and O_2 mole fraction in Ar or He. The electron-impact cross section data are taken from the data base discussed extensively by Phelps and co-workers.[11-13] The calculations and data base are discussed in detail in Ref. 8.

The rate coefficient for each electron-impact excitation process is given by the convolution integral of the energy-dependent excitation cross sections $\sigma(E)$ and the electron energy distribution N(E):

$$k = \left(\frac{2e}{m}\right)^{1/2} \int_o^\infty \sigma(E) N(E) E dE \qquad (4)$$

Cross sections for $O_2(a)$ excitation,[12] O_2 dissociation,[14] and O_2 ionization[13] are shown in Fig. 2. Although $O_2(a)$ lies at an energy of ~1 eV, its excitation cross section peaks at 6-7 eV. In addition, electron energies >12 eV are required to maintain ionization in the plasma. Thus the electron energy distribution or "temperature" must be "hot" enough to provide sufficient overlap with these cross sections. Clearly, an electron energy distribution which gives significant $O_2(a)$ excitation and ionization will also give substantial O-atom production.

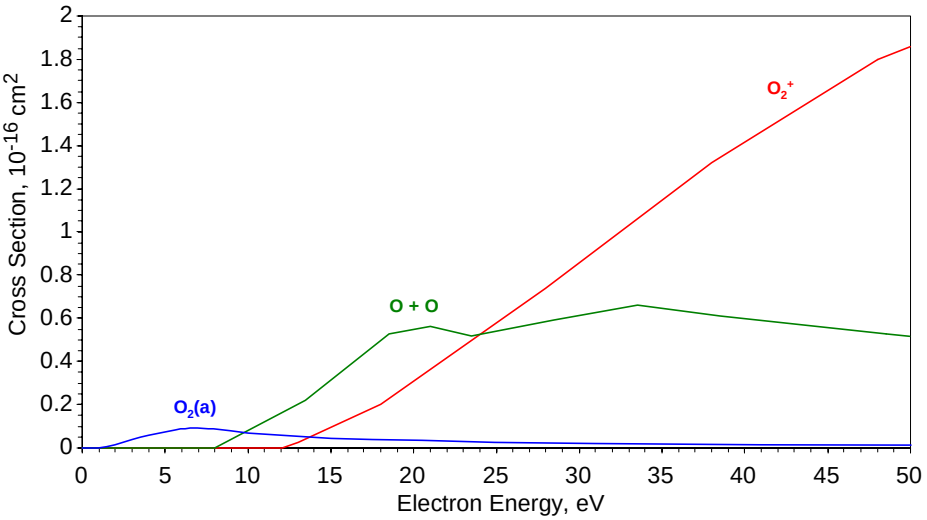

Figure 2: Cross sections for electron-impact excitation of O_2 to form $O_2(a)$, O + O, and O_2^+.

Two experimental controls on the electron energy distribution are the E/N of the discharge and the relative amounts of O_2 and rare gas (He or Ar) in the gas mixture. E/N is the ratio of the field strength E, governed by the applied power and discharge geometry, to the total number density N, governed by pressure and temperature. The effects of E/N and O_2 mole fraction on the computed electron energy distributions are shown in Fig. 3. With either increasing E/N or decreasing O_2 fraction, the fraction of high-energy electrons increases, signifying increasing electron "temperature". The increases in the high-energy component of the electron energy distribution result in larger overlap integrals with the key electronic excitation cross sections, illustrated in Fig. 4. The 10 Td distribution provides power-efficient $O_2(a)$ excitation, in that very little power is expended on O_2 dissociation; however the poor overlap with the ionization cross section results in a very low ionization rate and consequently low electron number density. The 100 Td distribution gives greater overlap with both the $O_2(a)$ excitation cross section and the O_2 ionization cross section, but at the expense of increased O_2 dissociation. The $O_2(a)$ excitation rate is given by the product $k_{exc}[e^-][O_2]$. Both k_{exc} and $[e^-]$, and hence the yield of $O_2(a)$, can be considerably enhanced through use of larger E/N and/or lower O_2 mole fraction to achieve more energetic electron energy distributions. This illustrates the basic conundrum of $O_2(a)$ generation for EOIL: high power utilization efficiency is optimized by "cold" electron energy distributions (e.g. lower E/N), however high $O_2(a)$ production rate and therefore high $O_2(a)$ yield require more energetic distributions (e.g. higher E/N).

The computed dependences of the rate coefficients for $O_2(a)$ excitation, O_2 dissociation, and O_2 ionization on O_2 mole fraction in Ar are shown in Fig. 5 for E/N = 50 Td. The excitation rate coefficient increases modestly with decreasing O_2 fraction. However, the O_2 ionization rate coefficient increases by almost two orders of magnitude from 80% O_2 to 5% O_2, signifying a large increase in the ion pair production rate and in the electron number density. The Ar ionization rate coefficient, which has a higher energy threshold, is even more sensitive to the O_2 fraction, and becomes an important contributor for the dilute mixtures.

For the low-power Evenson discharge configuration, the gas residence time in the discharge is ~0.2 ms. This corresponds to an effective $O_2(a)$ "loss" rate which is faster than the collisional losses within the discharge for our anticipated electron number densities. To zeroth order, we can approximate the $O_2(a)$ production as

$$[O_2(a)] \quad . \quad k_{exc}[e^-][O_2]\tau \quad , \qquad (5)$$

where τ denotes the gas residence time in the discharge. The $O_2(a)$ yield is then simply $\sim k_{exc}[e^-]\tau$, and is thus highly dependent on the electron energy distribution via E/N and O_2 fraction. The gas residence time in the 1 kW coaxial discharge is longer, ~4 ms, so a full treatment for that case requires inclusion of the $O_2(a)$ losses due to collisions with electrons (superelastic quenching, dissociation), as well as the effects of dissociative attachment of electrons with O_2 and the subsequent role of O^-.[15,16] (Note that deactivation of $O_2(a)$ by collisions with the reactor walls and with neutral discharge species in and downstream of the discharge is negligible for our experimental conditions.)

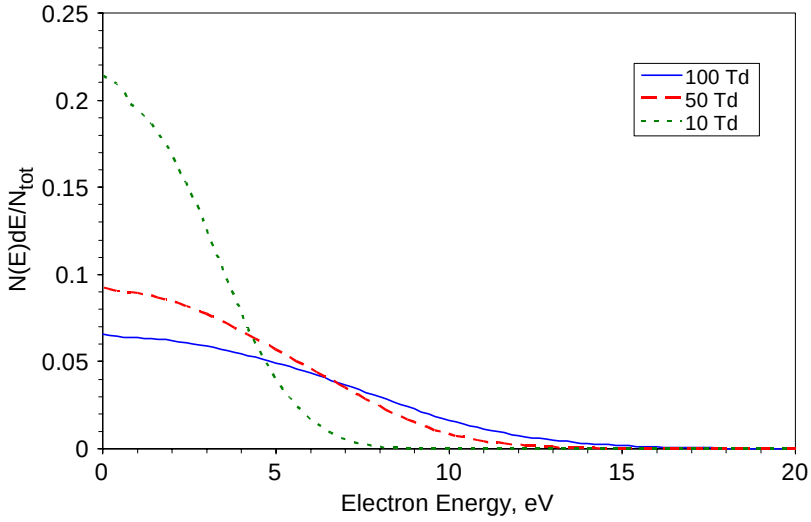

(a)

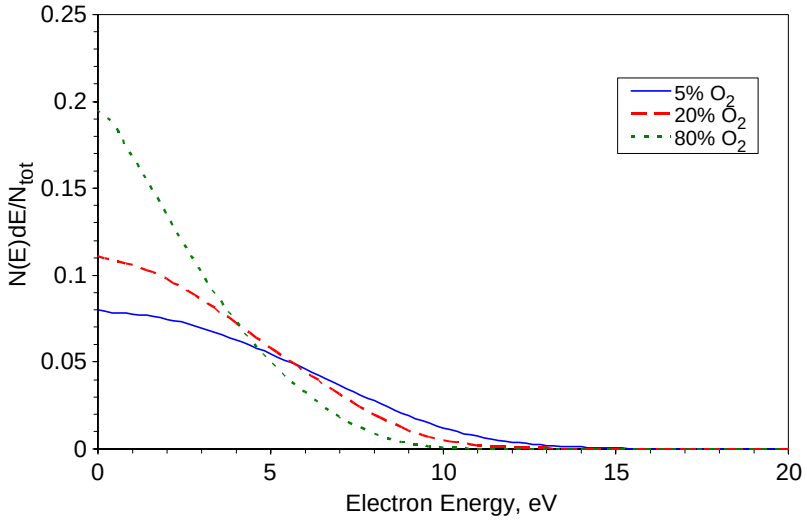

(b)

Figure 3: Computed electron energy distribution functions in discharge-excited O_2/Ar mixtures: (a) Effect of variations in E/N for 10% O_2 in Ar; (b) Effect of variations in O_2 mole fraction for E/N = 50 Td.

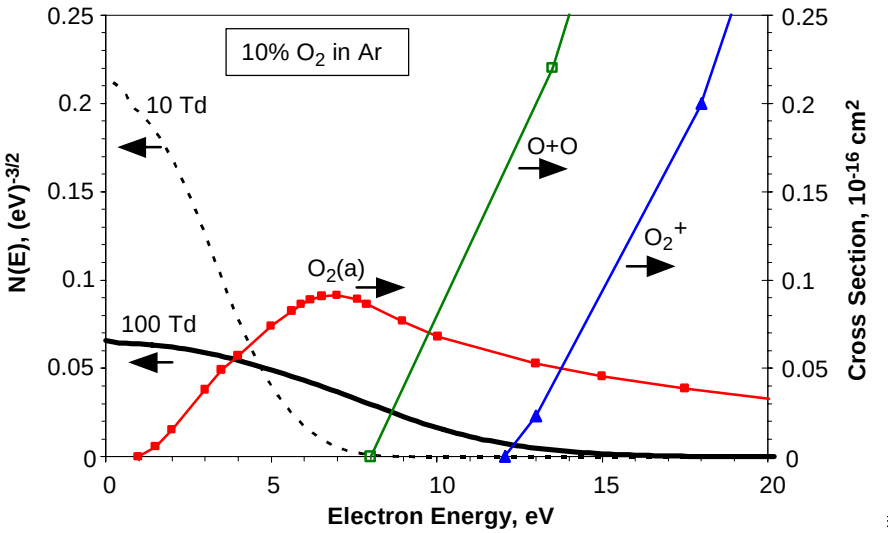

Figure 4: Illustration of overlap of electron energy distributions with electron impact excitation cross sections for $O_2(a)$ excitation, O_2 dissociation to form O + O, and O_2 ionization to form O_2^+. The electron energy distributions are computed for E/N = 10 and 100 Td, in 10% O_2/Ar.

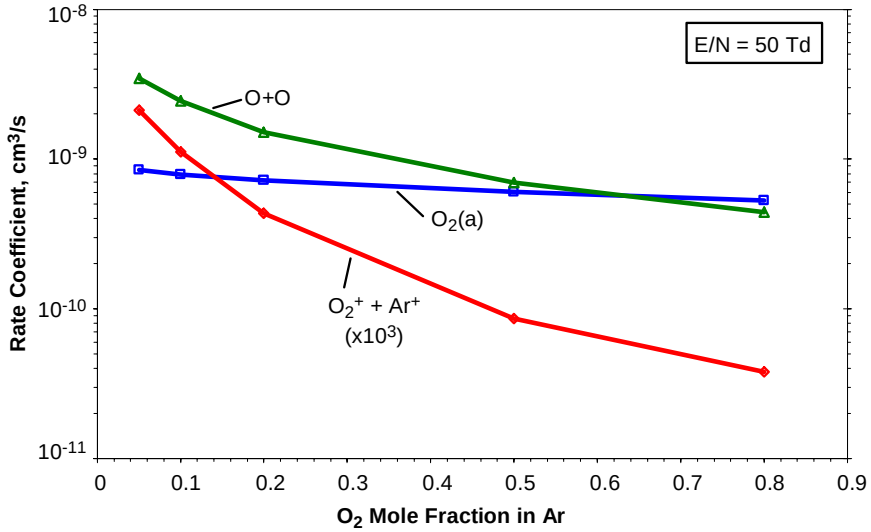

Figure 5: Effect of variations in O_2 mole fraction on computed electron-impact rate coefficients for $O_2(a)$ excitation, O_2 dissociation, and total ionization for discharge-excited O_2/Ar mixtures, E/N = 50 Td.

3. EXPERIMENT DESCRIPTION

Low-power, room-temperature experiments are performed in a conventional discharge-flow reactor shown in Fig. 6.[4,5,17] Experimental conditions are 5-80% O_2 in Ar at 1.5 and 3 torr (nominally 2 and 4 mmole/s, respectively), 40-120 W discharge power, E/N ~ 50-100 Td, 0.2 ms gas residence time in the discharge, flow velocities 1100-1300 cm/s in the 5 cm o.d. main flow tube, flow temperatures ~500 K in the discharge and ~350 K in the reaction zone. I_2 is added through the sliding injector to give variable reaction times of 4 to 15 ms. Typical initial (unreacted) species

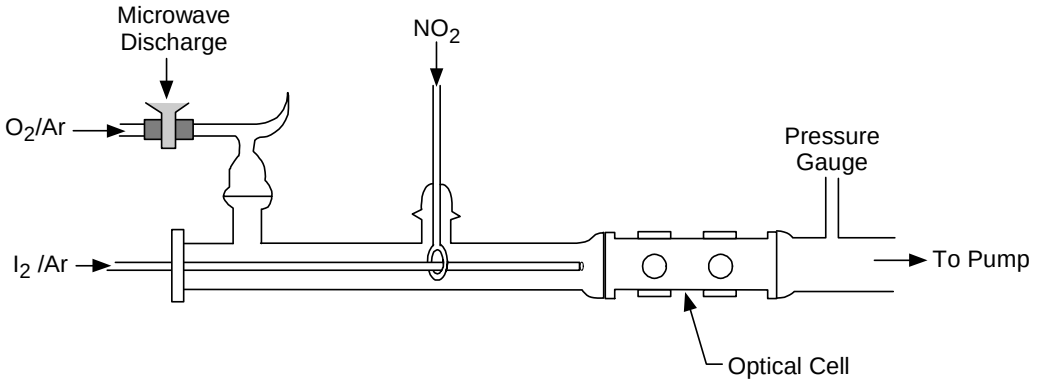

Figure 6: Schematic diagram of low-power, subsonic discharge-flow reactor apparatus.

concentrations are $[O_2(a)] \sim [O] \sim 10^{14\text{-}15}$ cm^{-3}, $[I_2] \sim 10^{13}$ cm^{-3}. NO_2 is added through a fixed-loop injector to reduce [O] to approximately the same as the initial $[I_2]$. Optical measurements of the key species include: $[O_2(a)]$ and [I*] by absolute emission spectroscopy at 1.27 and 1.315 μm; temperature, gain, and the quantity {[I*]-[I]/2} by tunable diode laser absorption spectroscopy at 1.315 μm; [O] by absolute air-afterglow photometry at 580 nm; and $[I_2]$ by ultrasensitive LED absorption photometry at 488 nm.[5,17] In this way, we fully constrain the EOIL reaction set by directly observing the concentrations of $O_2(a)$, I*, I, I_2, and O in the reaction zone, as well as the gas temperature.

High-power (1-2 kW), high-throughput experiments are performed on the supersonic discharge-flow reactor diagrammed in Fig. 7. The Microwave Driven Jet (or MIDJet) discharge plenum is illustrated in Fig. 8. O_2/He and O_2/I_2/He mixtures are injected into the plenum via a set of tangential jets to give a swirl flow that confines the discharge near the axis. The discharge effluent expands at M ~ 2 through a water-cooled boron nitride nozzle into the downstream flow section, where optical measurements of $[O_2(a)]$, [I*], [I], and T are performed as described above. Typical experimental conditions are 2-50% O_2 in He, plenum pressures 35-50 torr, total discharge gas flow rates 35-42 mmole/s, discharge power 1 kW, discharge temperature ~1000 K. For the more dilute O_2/He mixtures, our 400 cfm (air) pumping speed limits the supersonic expansion conditions to M = 1.8, T = 500 K, P = 7.5 torr, due to the relatively low pumping capacity for helium. The MIDJet device is capable of operation up to 5 kW discharge power, with proportionately higher gas flow rates to optimize the $O_2(a)$ production. All of the results presented here are for 1 kW discharge power and E/N ~ 30-43 Td.

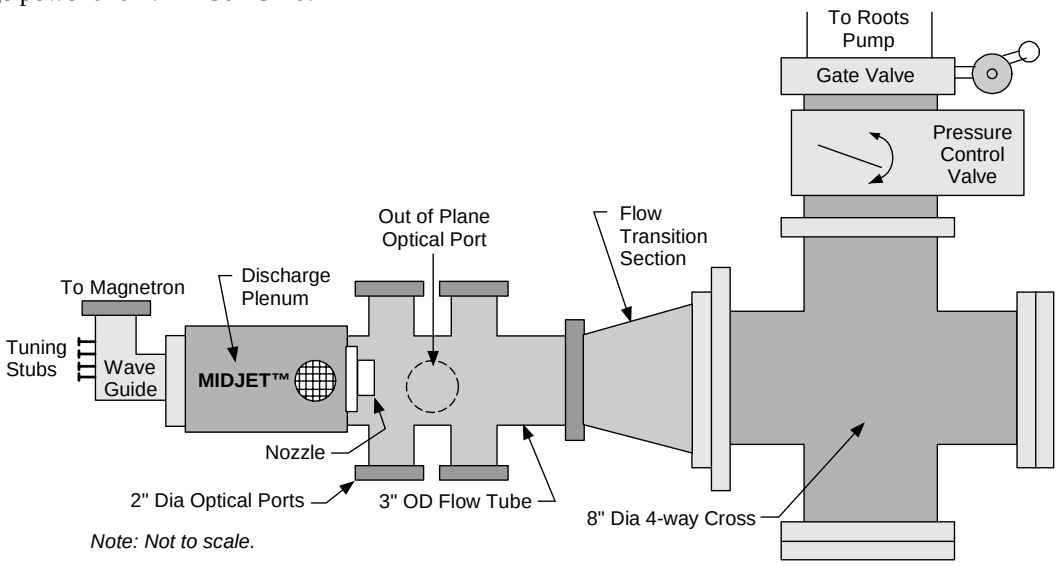

Figure 7: Diagram of high-power, supersonic discharge-flow reactor.

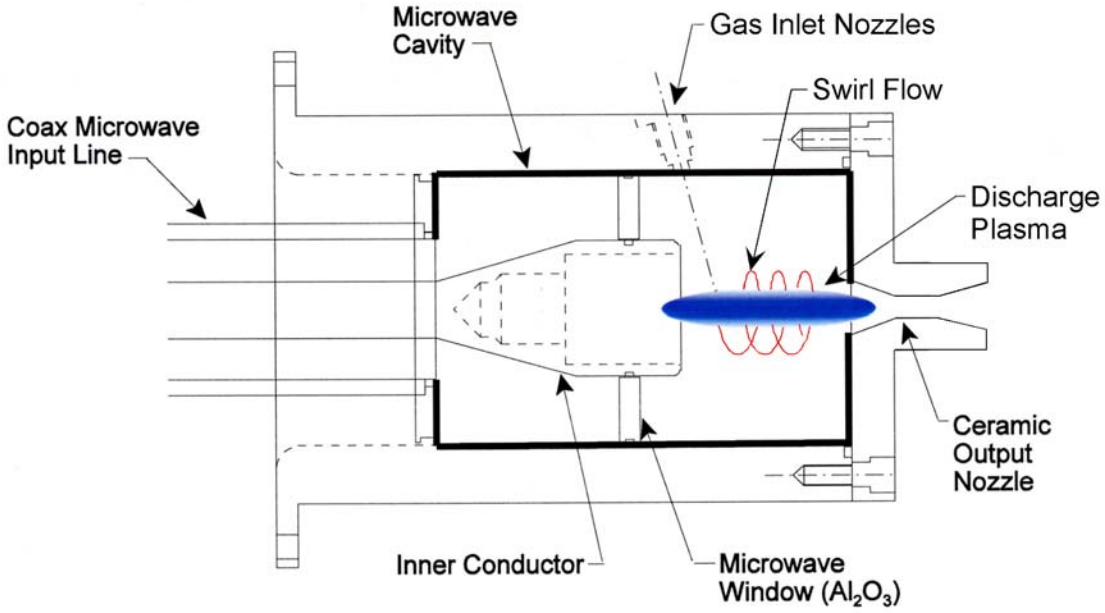

Figure 8: Diagram of 1-5 kW MIDJet discharge plenum.

4. EXPERIMENTAL RESULTS: $O_2(a)$ YIELDS

As expected from the discharge model described above, the yield of $O_2(a)$ increases dramatically as the mole fraction of O_2 is decreased. Results from the low-power subsonic reactor are shown in Figs. 9 and 10, illustrating the influence of power, pressure, and O_2 mole fraction on the $O_2(a)$ yields. Clearly, increases in E/N and in Ar content result in more energetic electron energy distributions, which in turn give larger $O_2(a)$ excitation rates and yields. While these parameters give some increase in the $O_2(a)$ rate coefficient, most of this effect is probably due to increased electron number densities as a result of increased ionization rates. We have found that, for ~5% O_2/Ar mixtures, it is easy to obtain 20-25% $O_2(a)$ yields at 70-100 W power and 1-3 torr. As shown in Fig. 1, these yields should be high enough to produce positive I*-I gain even at room temperature, and we have indeed observed positive gain at 350 K when using NO_2 to suppress atomic oxygen effects.[4,5] We have also quantified atomic oxygen yields from the low-power discharge, and have examined the complex quenching kinetics of I* which appear to be related to atomic oxygen processes. These results are reported in detail elsewhere.[5]

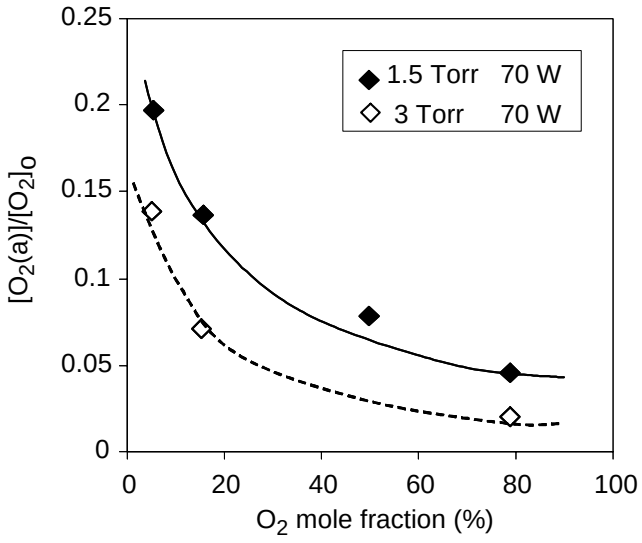

Figure 9: Dependence of $O_2(a)$ yield on O_2 mole fraction and total pressure: Ar diluent, 70 W discharge power, 1.5 and 3 torr.

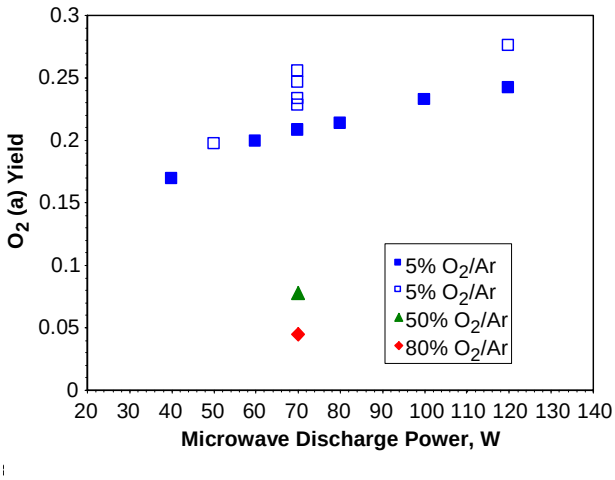

Figure 10: Dependence of $O_2(a)$ yield on microwave discharge power for 1.5 torr and three O_2/Ar mixtures. The two data sets for 5% O_2/Ar were observed on separate, consecutive days, and indicate day to day variability in the discharge operation.

The $O_2(a)$ yield results are remarkably similar for the 1 kW MIDJet discharge system. $O_2(a)$ and I* emission spectra from the supersonic flow for different discharge conditions are shown in Figs. 11 and 12. As the O_2 mole fraction is decreased by a factor of 4, the $O_2(a)$ emission intensity decreases by less than a factor of 2, signifying an increased yield. In addition, the I* emission intensity, proportional to [I*], is higher for the lower O_2 mole fractions, signifying more I* excitation due to larger $O_2(a)$ yield. Small signal gain measurements on the I*-I transition by the tunable diode laser diagnostic are shown in Fig. 13. The data show net absorption at ~500 K (the flow expansion and temperature are limited by low pumping speed for He), however the absorption decreases as the $O_2(a)$ yield increases. This signifies transfer of population from I to I*, commensurate with the behavior of the I* emission.

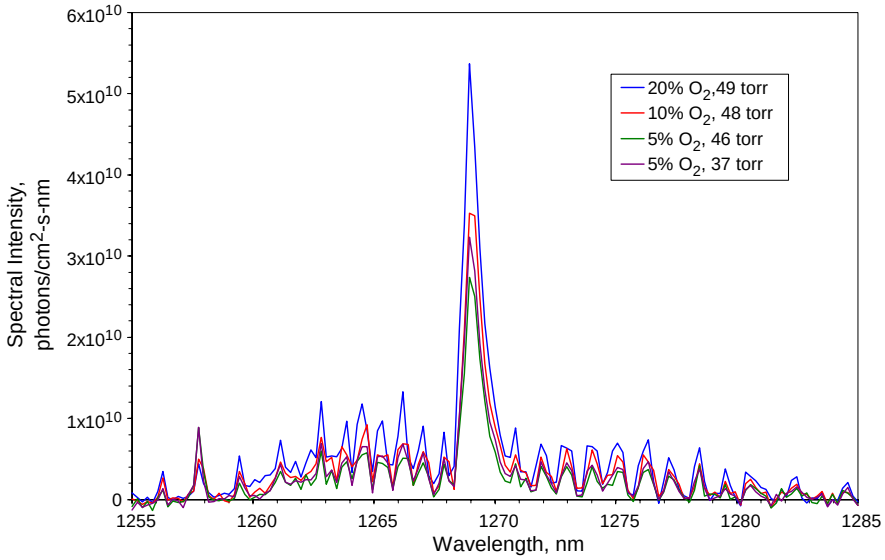

Figure 11: $O_2(a)$ emission spectra from 1 kW discharge, for different O_2 mole fractions at the plenum pressures indicated.

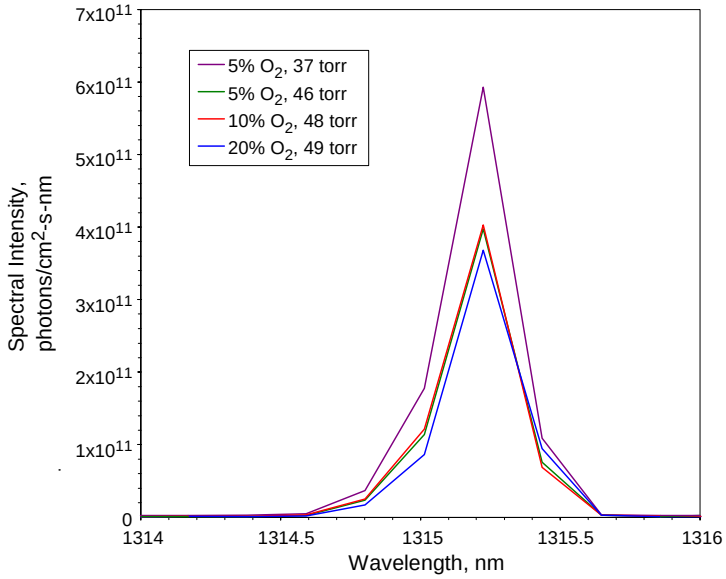

Figure 12: I* emission spectra for the conditions given in Figure 11, I_2 flow rate = 0.18 μmole/s

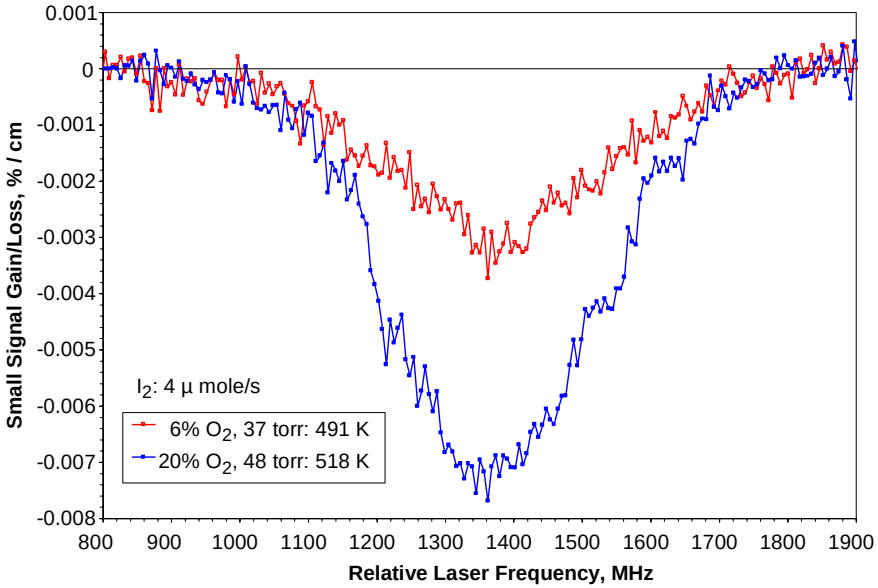

Figure 13: Atomic iodine absorption line shapes, 1 kW discharge power.

Through integration of the $O_2(a)$ emission spectra and application of the Einstein coefficient for the (a→X) transition, we determine $[O_2(a)]$ and hence the $O_2(a)$ yields.[4,5] The observed $O_2(a)$ concentrations range from (0.7 to 3) x 10^{15} molecules/cm^3 for total O_2 concentrations of (0.3 to 5) x 10^{16} molecules/cm^3 in the 7.5 torr flow. The $O_2(a)$ yields for the 1 kW MIDJet discharge system are plotted in Fig. 14. These yields are comparable to those we observe in the low-power system, and exceed 20% for O_2 mole fractions below 10%.

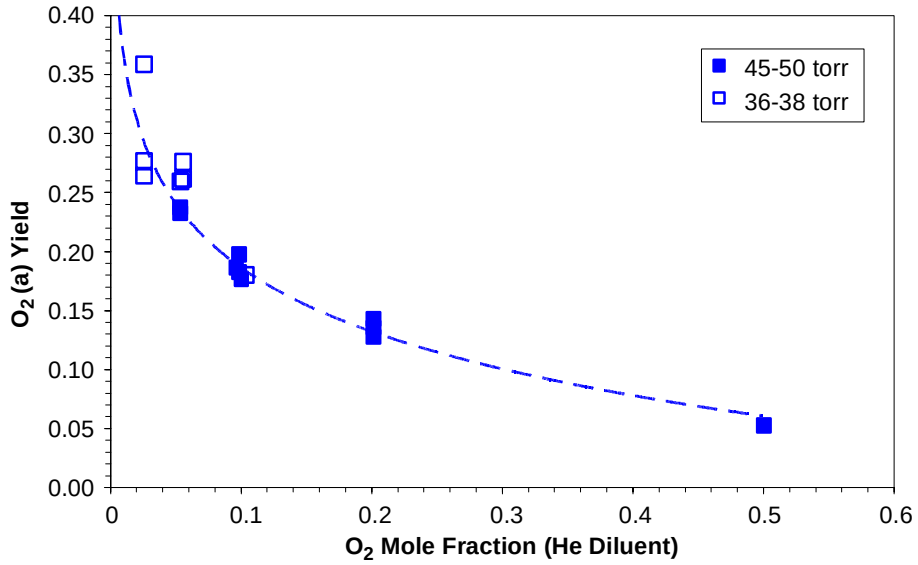

Figure 14: $O_2(a)$ yields generated by the PSI MIDJet discharge at 1 kW power. The dashed curve is a curvefit to the data at 45-50 torr.

5. ANALYSIS AND DISCUSSION

Using the data from the 1 kW MIDJet discharge, the product of the $O_2(a)$ yields and the total O_2 flow rates give the $O_2(a)$ flow rates plotted in Fig. 15. The total $O_2(a)$ power in the flow is indicated on the right hand axis. The $O_2(a)$ flow rates peak out at ~1 mmole/s, corresponding to a peak total $O_2(a)$ power of ~100 W and a peak power efficiency of ~10% for generation of $O_2(a)$, at an O_2 mole fraction of 20%. Using Eq. (3), we can evaluate the maximum power available for lasing, assuming a temperature in the cavity as produced by supersonic expansion. We use a curvefit to represent our observed values of Y_Δ versus O_2 mole fraction for 1 kW discharge power, 45-50 torr in the discharge plenum, and supersonic flow temperatures of 180, 200, and 250 K. The results are shown in Fig. 16. The available $O_2(a)$ powers above the gain threshold are substantial: 10 to 50 W with maxima at O_2 mole fractions of 10-15%. Note that these values are not projections or model predictions, but are derived directly from the actual $O_2(a)$ yields observed in the 1 kW discharge experiments. Since the observed yields are comparable to those we previously used to demonstrate positive gain near room temperature,[4] and are substantially larger than those used in previous EOIL laser demonstrations in supersonic flow,[2,3] it is clear that the order of tens of watts of laser power could be extracted from this 1 kW discharge system with sufficient pumping capacity to adequately cool the flow. We estimate that this could be accomplished with a pumping speed of at least 2000 cfm (air).

For discharge operation at kW and higher powers, heat deposition and the temperature of the plenum gas are significant issues. Simple physics dictates that the temperature rise due to heat deposition from the applied discharge power should scale as the ratio of the power to the molar (or mass) flow rate of the gas. If there were no active cooling of the MIDJet plenum, the temperature rise would be ~1275 K for 1 kW power. However, for the present water-cooled system, we observe $\Delta T \sim 700$ K. Nevertheless, this results in a plenum gas temperature of 1000 K, which necessitates a Mach number $M > 3$ to reach $T < 250$ K in the supersonic expansion. Thus an important aspect of the design of future high-power EOIL systems will be to implement aggressive active cooling of the plenum gas, preferably to temperatures below ~800 K so that Mach 2-3 nozzles can be used.

The microwave discharge technology offers promise for scaling to higher discharge powers and hence higher laser output powers. The device described here is capable of operation up to 5 kW discharge power. High power magnetrons in the 100 kW class are commercially available. As the power is increased, the total gas flow rate is increased by a roughly proportional amount. So if the high $O_2(a)$ yields can be maintained under these conditions, then the total $O_2(a)$ power and the power available above threshold should also scale accordingly.

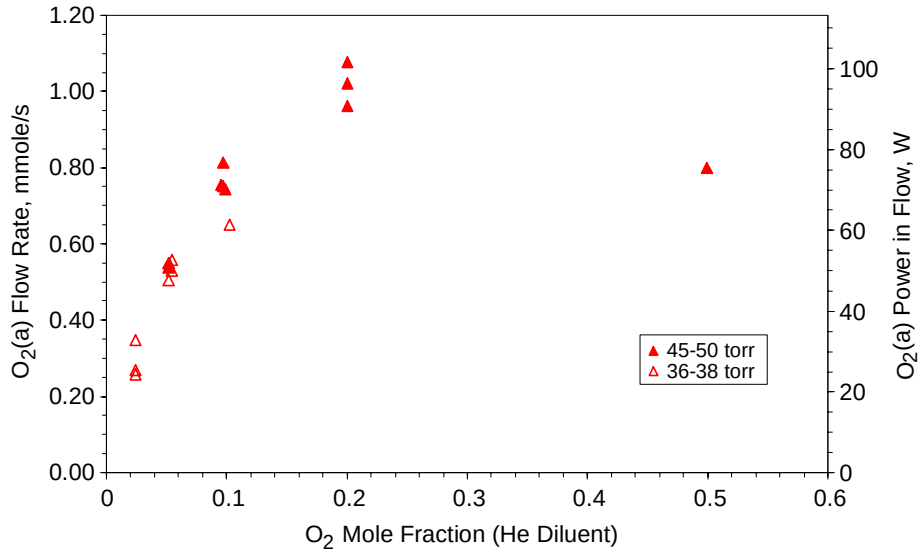

Figure 15: $O_2(a)$ molar flow rates generated by the PSI MIDJet discharge at 1 kW power. Total $O_2(a)$ power in the flow is indicated on the right hand axis.

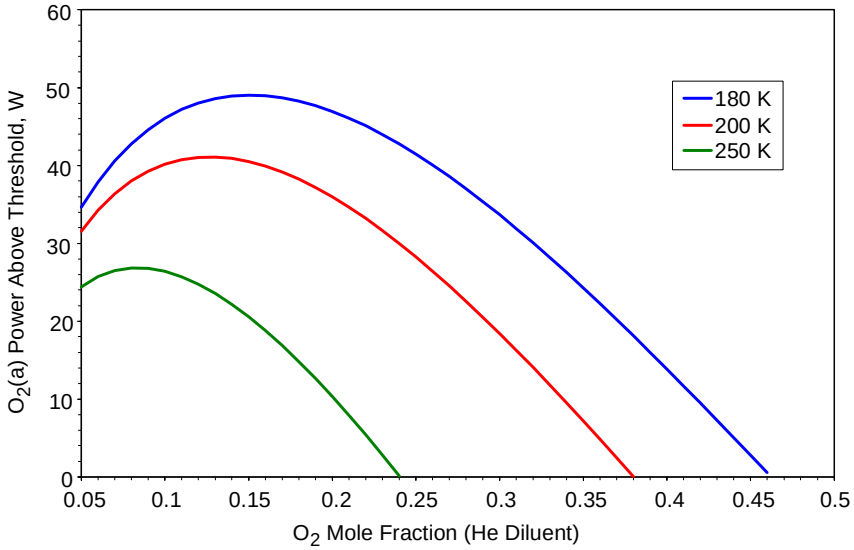

Figure 16: $O_2(a)$ power available in the flow (above threshold) for selected flow temperatures, corresponding to the observed MIDJet $O_2(a)$ yields at 1 kW discharge power, 45-50 torr plenum pressure

Our current data at 1 kW indicate a power/flow rate ratio corresponding to about 25 to 30 kJ/mole (including the helium diluent), or about 1 to 5 eV per oxygen molecule. Although this factor needs to be more precisely determined through flow rate optimization as a function of O_2/He ratio, it is consistent with the electron energies required to excite $O_2(a)$ as shown by the cross section plotted in Fig. 2. These approximate scaling considerations indicate that at least 1 kW of potential laser power (available power above threshold) can be achieved with the 30 kW discharge source.

The data presented here are too limited in scope to permit conclusive estimates of the "wall plug" efficiency for a high-power EOIL system. However, we note that the maximum efficiency implied by our 1 kW experiments is ~10% for $O_2(a)$ production and a few per cent for potential laser output. The ultimate efficiency at elevated power depends on a complex interplay of several factors which we have not yet tried to optimize: power/flow rate ratio, trade-offs between

$O_2(a)$ yield and oxygen flow rate, discharge ionization rate, discharge plenum temperature and pressure, supersonic expansion characteristics, O-atom effects, I_2 injection and mixing dynamics, optical power extraction requirements, etc. For example, if engineering improvements can reduce the power/flow rate ratio to ~1 eV/O_2 molecule with $O_2(a)$ yields similar to those reported here, then application of Eq. (3) indicates that laser power efficiencies up to 10% to 20% may be feasible. In addition, commercial microwave systems at 30 kW and higher operate at much lower frequencies, e.g. 915 MHz at 30 kW, enabling larger discharge volume and larger diameter for the supersonic expansion orifice and further reducing the power/flow rate ratio for a given plenum pressure. The availability of these kW-class microwave power sources provides an avenue for systematic examination of these factors.

ACKNOWLEDGEMENTS

The authors appreciate many stimulating discussions with Wayne Solomon at University of Illinois Urbana-Champaign, David Carroll and Joseph Verdeyen at CU Aerospace, Michael Heaven at Emory University, Glenn Perram at the Air Force Institute of Technology, Gordon Hager and Timothy Madden at the Air Force Research Laboratory, and B. David Green and George Caledonia at Physical Sciences Inc. Michael Read contributed to the design and analysis of the high-power microwave system. The 1 kW $O_2(a)$ experiments were supported by the U.S. Air Force Research Laboratory, Kirtland AFB, Contract FA9451-04-M-0239, Dr. Kevin Hewett, COTR. The remainder of this research was funded by the Air Force Office of Scientific Research through a Multidisciplinary Research Initiative, prime contract F49620-01-1-0357, Dr. Michael Berman, contract monitor.

REFERENCES

1. D.L. Carroll, J.T. Verdeyen, D.M. King, J.W. Zimmerman, J.K. Laystrom, B.S. Woodard, N. Richardson, K. Kittell, M.J. Kushner, and W.C. Solomon, "Measurement of Positive Gain on the 1315 nm Transition of Atomic Iodine Pumped by $O_2(a^1\Delta)$ Produced in an Electric Discharge," Appl. Phys. Lett. 85, 1320-1322 (2004).
2. D.L. Carroll, J.T. Verdeyen, D.M. King, J.W. Zimmerman, J.K. Laystrom, B.S. Woodard, G.F. Benavides, K. Kittell, D.S. Stafford, M.J. Kushner, and W.C. Solomon, "Continuous-Wave Laser Oscillation on the 1315 nm Transition of Atomic Iodine Pumped by $O_2(a^1\Delta)$ Produced in an Electric Discharge," Appl. Phys. Lett. 86, 111104 (2005).
3. D.L. Carroll, J.T. Verdeyen, D.M. King, J.W. Zimmerman, J.K. Laystrom, B.S. Woodard, G.F. Benavides, K. Kittell, and W.C. Solomon, "Path to the Measurement of Positive Gain on the 1315-nm Transition of Atomic Iodine Pumped by $O_2(a^1\Delta)$ Produced in an Electric Discharge," IEEE J. Quantum Electron. 41, 213-223 (2005).
4. W.T. Rawlins, S. Lee, W.J. Kessler, and S.J. Davis, "Observations of Gain on the $I(^2P_{1/2} \rightarrow {}^2P_{3/2})$ Transition by Energy Transfer from $O_2(a^1\Delta_g)$ Generated by a Microwave Discharge in a Subsonic Flow Reactor," Appl. Phys. Lett. 86, 051105 (2005).
5. W.T. Rawlins, S. Lee, W.J. Kessler, L.G. Piper, and S.J. Davis, "Advanced Diagnostics and Kinetics of Oxygen-Iodine Laser Systems," AIAA-2005-5299, 36th AIAA Plasmadynamics and Lasers Conference, Toronto, Ontario, Canada, June 2005.
6. F.C. Fehsenfeld, K.M. Evenson, and H.P. Broida, "Microwave Discharge Cavities Operating at 2450 MHz," Rev. Sci. Instrum. 36, 294-298 (1965).
7. Kaufman, F., "The Production of Atoms and Simple Free Radicals in Glow Discharges," *Adv. Chem. Ser.* **80**, 29-47 (1969).
8. Rawlins, W.T., Caledonia, G.E., and Armstrong, R.A., "Dynamics of Vibrationally Excited Ozone Formed by Three-Body Recombination. II. Kinetics and Mechanism," *J. Chem. Phys.* **87**, 5209-5221 (1987).
9. W.L. Morgan and B.M. Penetrante, "ELENDIF: A Time-Dependent Boltzmann Solver for Partially Ionized Plasmas," Computer Physics Communications 58, 127-152 (1990).
10. Frost, L.S. and Phelps, A.V., "Momentum-Transfer Cross Sections for Slow Electrons in He, Ar, Kr, and Xe from Transport Coefficients," *Phys. Rev. A* **136**, 1538 (1969).
11. Lawton, S.A., and Phelps, A.V., "Excitation of the $b^1\Sigma_g^+$ State of O_2 by Low Energy Electrons," *J. Chem. Phys.* **69**, 1055 (1978).

12. Tachibana, K., and Phelps, A.V., "Excitation of the O_2 ($a^1\Delta_g$) State by Low Energy Electrons," *J. Chem. Phys.* **75**, 3315 (1981).
13. A.V. Phelps, private communication, ftp://jila.colorado.edu/collision_data/.
14. P.C. Cosby, "Electron-Impact Dissociation of Oxygen," J. Chem. Phys. 98, 9560-9569 (1993).
15. R.N. Franklin, "The Role of $O_2(a^1\Delta_g)$ Metastables and Associative Detachment in Discharges in Oxygen," J. Phys. D: Appl. Phys. 34, 1834-1839 (2001).
16. D.S. Stafford and M.J. Kushner, "$O_2(^1\Delta)$ Production in He/O_2 Mixtures in Flowing Low Pressure Plasmas," J. Appl. Phys. 96, 2451-2465 (2004).
17. W.T. Rawlins, S. Lee, W.J. Kessler, D.B. Oakes, L.G. Piper, and S.J. Davis, "Spectroscopic Studies of a Prototype Electrically Pumped COIL System," SPIE **5334**, Paper No. 12 (2004).